



OPEN ACCESS

EDITED BY

Chuanyou Li,
Institute of Geology, China Earthquake
Administration, China

REVIEWED BY

Lichun Chen,
Guilin University of Technology, China
Xuhua Shi,
Zhejiang University, China

*CORRESPONDENCE

Xingwang Liu,
lxw_27@163.com

SPECIALTY SECTION

This article was submitted to Structural
Geology and Tectonics,
a section of the journal
Frontiers in Earth Science

RECEIVED 12 May 2022

ACCEPTED 04 August 2022

PUBLISHED 30 August 2022

CITATION

Liu X, Gao Z, Lei Q, Shao Y and Yao Y
(2022), Timing of Paleoeearthquakes and
Seismic Hazard of the Zhuozishan West
Piedmont Fault in the Northwestern
Ordos Block.
Front. Earth Sci. 10:942242.
doi: 10.3389/feart.2022.942242

COPYRIGHT

© 2022 Liu, Gao, Lei, Shao and Yao. This
is an open-access article distributed
under the terms of the [Creative
Commons Attribution License \(CC BY\)](#).
The use, distribution or reproduction in
other forums is permitted, provided the
original author(s) and the copyright
owner(s) are credited and that the
original publication in this journal is
cited, in accordance with accepted
academic practice. No use, distribution
or reproduction is permitted which does
not comply with these terms.

Timing of Paleoeearthquakes and Seismic Hazard of the Zhuozishan West Piedmont Fault in the Northwestern Ordos Block

Xingwang Liu^{1,2*}, Zemin Gao³, Qiyun Lei⁴, Yanxiu Shao⁵ and Yunsheng Yao^{1,2}

¹Gansu Lanzhou Geophysics National Observation and Research Station, Lanzhou, China, ²Lanzhou Institute of Geotechnique and Earthquake, China Earthquake Administration, Lanzhou, China, ³Faculty of Geoscience and Environmental Engineering, Southwest Jiaotong University, Chengdu, China, ⁴Earthquake Agency of Ningxi Hui Autonomous Region, Yinchuan, China, ⁵Institute of Surface-Earth System Science, Tianjin University, Tianjin, China

The Zhuozishan West Piedmont Fault (ZWPF) is an active normal fault in the northwestern corner of the Ordos Block. Studying the recurrence characteristics of paleoeearthquakes is useful for understanding the regional seismic hazard potential. In this study, paleoseismic trench and optically stimulated luminescence (OSL) dating methods are used to determine the temporal sequence of paleoeearthquakes. Seven earthquakes were constrained to be E7 (73.4 ± 12.9 ka to 75.3 ± 10.6 ka), E6, (63.7 ± 7.4 ka to 64.4 ± 8.2 ka), E5 (53.2 ± 7.0 ka to 58.7 ± 6.5 ka), E4 (42.6 ± 6.3 ka to 47.7 ± 5.8 ka), E3 ($31.0-3.4$ ka to 31.3 ± 3.4 ka), E2 (26.1 ± 2.7 ka to 28.1 ± 3.8 ka) and E1 (15.8 ± 1.9 ka to 20.2 ± 2.6 ka). The recurrence interval of strong earthquakes in the ZWPF is roughly constrained to be 8.1–14 ka, with magnitudes of Mw 7.0–7.4 that ruptured the entire fault. Based on the timing of the latest earthquake event, the elapsed time approached or exceeded the recurrence interval revealed from paleoeearthquakes. Hence, we suggest that the northwestern corner of the Ordos Block has a significantly high seismic hazard potential and that the occurrence of a strong earthquake should not be underestimated.

KEYWORDS

zhuozishan west piedmont fault, ordos block, normal fault, paleoseismic event, seismic hazard

Introduction

The boundary zone of Ordos Block are composed of normal faults and affected by regional large scale active faults, which are capable of generating strong earthquakes, which are one of the important strong seismic fault zones in China ([Research Group of Active Fault System around Ordos Massif, 1988](#)). Many earthquakes with $M \geq 8$, such as the Baotou earthquake in 849 ([Research Group of Active Fault System around Ordos Massif, 1988](#); [Jiang et al., 2000](#); [Nie et al., 2010](#); [Li et al., 2015](#)), the Hongdong earthquake

in 1303 (Meng et al., 1985; Jiang et al., 2004; Xu et al., 2018), the Huaxian earthquake in 1556 (Rao et al., 2015; Ma et al., 2016; Du et al., 2017; Feng et al., 2020), the Pingluo earthquake in 1739 (Zhang et al., 1986; Deng and Liao, 1996; Lin et al., 2013; Middleton et al., 2016) and the Haiyuan earthquake in 1920 (Deng et al., 1984; Zhang et al., 1988; Ren et al., 2016; Ou et al., 2020), have occurred within these basin systems and have caused severe casualties and economic losses (Figure 1). Research on active faults and seismic hazard assessment are important for reducing earthquake disasters.

Paleoearthquakes are related to prehistoric earthquake events preserved in geological records or events that were not recorded in history (Ran and Deng, 1999; Deng, 2002; Liu et al., 2021). The advantage of paleoseismic research is to compensate the

shortcomings and limitations of instruments and historical seismic records to a great extent so that we can understand the long-term activity and behavior of faults and estimate the hazard of future earthquakes over the period of several repeated earthquake cycles. In this study, we present field trench evidence for the occurrence of paleoearthquakes along the Zhuozhishan West Piedmont Fault (ZWPF) in the northwestern corner of the Ordos Block (Figures 1, 2). In the study area, there is a lack of earthquakes with $M \geq 7$ recorded by historical and instrumental recordings. Therefore, we attempt to enrich data of paleoearthquakes by optically stimulated luminescence (OSL) dating in an investigation of the timing and recurrence intervals of large earthquakes during the Pleistocene along the ZWPF. Our results of paleoseismological analysis are important for assessing

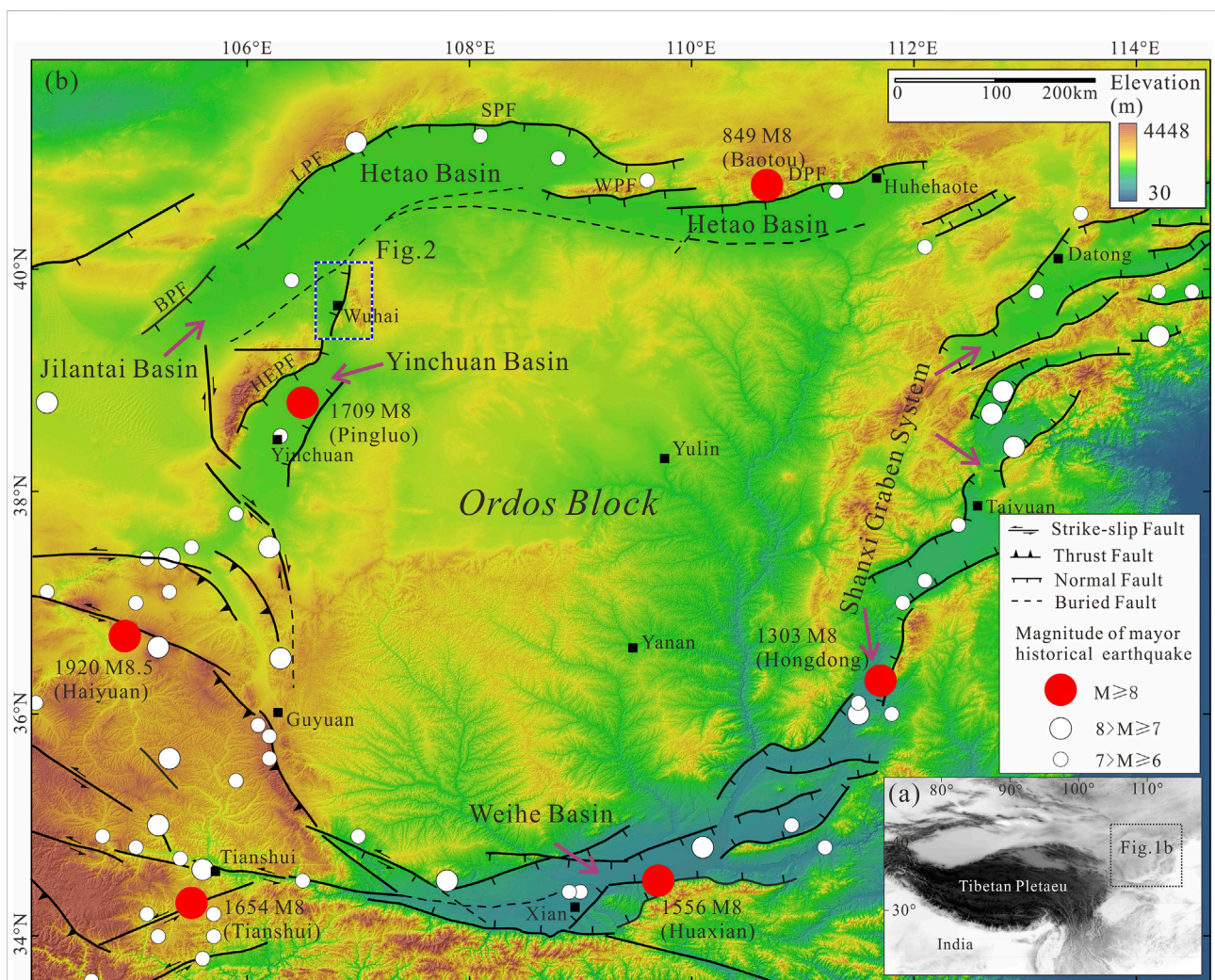


FIGURE 1
(A) Location of the Ordos Block. **(B)** Color-shaded relief map showing the distribution of large historical earthquakes and major active faults around the Ordos Block. The blue dashed rectangle shows the location of Figure 2. Abbreviations of names of active faults: DPF, Daqingshan Piedmont Fault; WPF, Wulashan Piedmont Fault; SPF, Seertengshan Piedmont Fault; LPF, Langshan Piedmont Fault; BPF, Bayanwulashan Piedmont Fault; HEPF, Helanshan East Piedmont Fault.

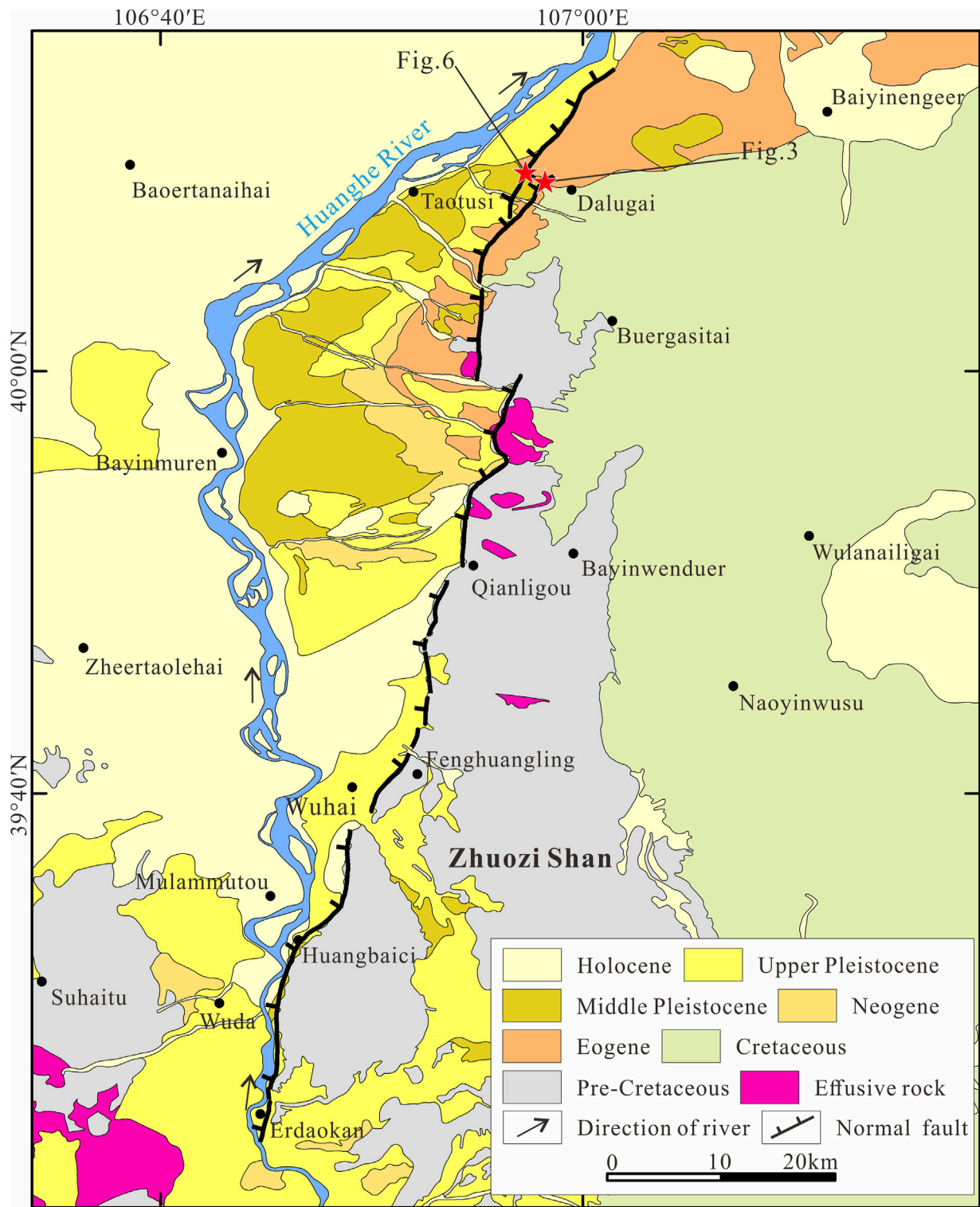


FIGURE 2 Geological map of the study area and its adjacent region, showing the distribution of bedrock lithology and the Zhuozishan West Piedmont Fault.

the seismic hazard in the northwestern corner of the Ordos Block and for a better general understanding of the seismogenic characteristics of normal faults in active basins.

Geological background

The Ordos Block, located in the western North China Craton, is a rigid block that has played an important role in tectonic activities in the Cenozoic in China (Research Group of Active Fault System around Ordos Massif, 1988; Zhang et al., 2002, 2003). There are no large-scale active faults developed within Ordos Block. It has good integrity and no records of earthquakes with a magnitude greater than M6 (Research Group of Active Fault System around Ordos Massif, 1988; Zhang et al., 2013), indicating the block is internally stable. However, there are series of large faulted basins controlled by active normal faults developed along the Ordos Block margin (Figure 1). A large number of studies have shown that regional tectonic activity and strong earthquakes mainly occur on active crustal block boundaries (Zhang et al., 2003; Zhang et al., 2004; Zhang et al., 2013; Zheng et al., 2020). According to historical data, more than 10 earthquakes with $M \geq 7$ have occurred around the Ordos Block, including five earthquakes with $M \geq 8$ (Research Group of Active Fault System around Ordos Massif, 1988; Jiang et al., 2000; Zhang et al., 2003). Therefore, the fault activities around the Ordos Block have always been the focus of active fault research (Research Group of Active Fault System around Ordos Massif, 1988; Jiang et al., 2000; Rao et al., 2015, 2016, 2018; Middleton et al., 2016; Dong et al., 2018; Xu et al., 2018; Zheng et al., 2019; Yu et al., 2021).

The study area is located in the northwestern corner of Ordos Block. A series of basins are developed in this area, including the Yinchuan Basin, the Jilantai Basin and the Hetao Basin (Research Group of Active Fault System around Ordos Massif, 1988) (Figure 1B). These basin boundaries are controlled by active normal faults that have caused destructive earthquakes. As the eastern boundary of the Yinchuan Basin, the Helanshan East Piedmont Fault (HEPF) is the seismogenic fault of the Pingluo M8 earthquake in 1739 (Zhang et al., 1986; Deng and Liao, 1996; Lin et al., 2013; Middleton et al., 2016). Previous studies suggested that the Daqingshan Piedmont Fault was the seismogenic fault of the Baotou M8 earthquake in 849 in the Hetao Basin (Research Group of Active Fault System around Ordos Massif, 1988; Jiang et al., 2000; Nie et al., 2010; Li et al., 2015). Another historical strong earthquake in the basin, an earthquake with a magnitude of nearly 8 in 7 BC, is considered to have occurred on the Langshan Piedmont Fault (LPF) (Li et al., 2015; Rao et al., 2016). There are also many paleoseismic records on the Sertengshan Piedmont Fault (SPF) and the Wulashan Piedmont Fault (WPF) (Yang et al., 2002, Yang et al., 2003; Chen et al., 2003; He et al., 2020). However, there are no records of

strong earthquakes and systematic studies of paleoearthquakes in the Jilantai Basin.

AS eastern boundary of the Jilantai Basin, the ~90-km-long NNE–SSW-trending Zhuozishan West Piedmont Fault (ZWPF) starts from the southeastern part of Dengkou County; extends southward by Dalugai, Qianligou, Fenghuangling, Wuhai, and Huangbaici; and terminates at Erdaokan from north to south, with dips ~50°–80° to the WNW (Figure 2). The fault traces are discontinuous and composed of several segments (Gao, 2020). If a strong earthquake occurs on the ZWPF, it will cause serious damages and losses to the Wuhai city. However, research on the ZWPF mainly focuses on the slip rate, the paleoseismic sequence and recurrence characteristics have not been studied (Zhang et al., 2014; Liang et al., 2019).

Materials and methods

Paleoseismic trenching has been the most effective method to study paleoearthquakes (Ran and Deng, 1999; McCalpin, 2009; Liu et al., 2021). In the exploration trench, the deformed strata and fault traces caused by strong earthquakes could be recorded. To identify normal fault paleoseismic events, colluvial wedges, filling wedges, and sudden changes in the displacement of different stratigraphic units are usually used as indicators (Deng et al., 1984; McCalpin, 2009; Ran et al., 2014). According to the recurrence model and evolution of paleoearthquakes along normal faults (McCalpin, 2009; Ran et al., 2014; Liu et al., 2021), after an earthquake, the fault scarp may collapse and result in the deposition of loose gravels, which finally become a colluvial wedge or filling wedges. Therefore, the fault planes together with the observed colluvial or filling wedges suggest an earthquake event. In the trenches we excavated, many colluvial or filling wedges are observed, which are the key indicators to identify paleoseismic events. Dating of the sediments below and overlying the wedges can be used to determine the lower and upper bound ages of paleoearthquakes (Ran and Deng, 1999; McCalpin, 2009; Ran et al., 2014; Liu et al., 2021).

Through remote sensing image interpretation and field investigation, we excavated three trenches near the Dalugai site along the northern segment of the ZWPF (Figure 2). Before excavation, we obtained high-resolution digital elevation model (DEM) data by using the structure from motion (SfM) technique for the study site (Bemis et al., 2014; Bi et al., 2017). Moreover, the SfM technique was also used to obtain photo mosaics of trench walls (Bemis et al., 2014; Gao et al., 2017).

To constrain the timing of paleoseismic events, OSL samples were collected from the sedimentary strata deposited before and after earthquakes, which can offer a time interval for the events (McCalpin, 2009; Ran et al., 2014). The dating was performed at the Laboratory of Neotectonic

TABLE 1 Result of OSL analysis for the layers in the trench.

	Depth (m)	U-238 (Bq/Kg)	Th-232 (Bq/Kg)	K-40 (Bq/Kg)	Dose rate (Gy/ka)	Equivalent dose (Gy)	OSL age (ka)
ZZS-OSL-11	5.0	25.4 ± 0.3	35.8 ± 4.3	607.1 ± 1.8	3.3 ± 0.1	229.8 ± 32.9	73.4 ± 12.9
ZZS-OSL-12	4.6	28.3 ± 1.4	21.7 ± 5.0	535.2 ± 0.4	2.7 ± 0.1	206.0 ± 19.8	75.3 ± 10.6
ZZS-OSL-13	4.1	49.0 ± 8.4	37.8 ± 3.1	554.6 ± 8.7	3.5 ± 0.1	222.4 ± 16.6	64.4 ± 8.2
ZZS-OSL-14	3.8	29.8 ± 1.2	31.1 ± 1.3	503.0 ± 1.4	3.1 ± 0.1	196.5 ± 10.4	63.7 ± 7.4
ZZS-OSL-18	0.6	45.5 ± 2.2	42.4 ± 3.1	503.8 ± 7.2	3.6 ± 0.1	56.4 ± 3.5	15.8 ± 1.9
ZZS-OSL-19	1.6	33.6 ± 2.5	37.0 ± 5.4	528.6 ± 9.2	3.3 ± 0.1	384.1 ± 23.8	117.0 ± 14.0
ZZS-OSL-20	0.9	38.7 ± 2.1	38.3 ± 2.2	456.8 ± 1.6	3.2 ± 0.1	290.4 ± 80.5	91.1 ± 26.9
ZZS-OSL-21	2.4	95.4 ± 1.0	88.6 ± 2.7	505.3 ± 10	4.5 ± 0.1	213.7 ± 13.6	47.7 ± 5.8
ZZS-OSL-22	2.0	59.1 ± 1.6	54.5 ± 1.0	536.2 ± 6.4	4.2 ± 0.1	178.7 ± 19.1	42.6 ± 6.3
ZZS-OSL-23	3.2	46.8 ± 1.3	46.9 ± 2.9	516.3 ± 3.2	3.6 ± 0.1	210.7 ± 8.4	58.7 ± 6.5
ZZS-OSL-24	2.8	75.6 ± 0.6	70.7 ± 1.4	638.1 ± 4.7	4.2 ± 0.1	224.1 ± 18.2	53.2 ± 7.0
ZZS-OSL-25	0.8	45.7 ± 1.0	41.7 ± 4.7	529.0 ± 5.8	3.6 ± 0.1	219.9 ± 20.6	61.1 ± 8.5
ZZS-OSL-26	0.4	39.1 ± 1.7	38.9 ± 1.5	532.9 ± 7.2	3.5 ± 0.1	211.9 ± 6.8	60.8 ± 6.5
ZZS-OSL-27	3.5	60.1 ± 2.3	41.7 ± 2.1	556.5 ± 11	3.8 ± 0.1	122.9 ± 10.1	32.3 ± 4.3
ZZS-OSL-28	3.2	50.9 ± 0.9	50.4 ± 1.1	544.9 ± 5.6	3.9 ± 0.1	122.2 ± 4.3	31.0 ± 3.4
ZZS-OSL-31	1.9	43.1 ± 1.2	32.7 ± 5.5	534.0 ± 0.6	3.2 ± 0.1	90.8 ± 8.1	28.1 ± 3.8
ZZS-OSL-32	1.6	50.1 ± 2.1	48.1 ± 1.9	506.3 ± 3.2	3.8 ± 0.1	81.3 ± 1.4	21.2 ± 2.2
ZZS-OSL-33	1.2	84.8 ± 0.9	76.3 ± 1.8	534.9 ± 5.8	4.3 ± 0.1	87.4 ± 6.5	20.2 ± 2.6
ZZS-OSL-36	2.6	39.1 ± 0.5	33.9 ± 3.4	539.0 ± 3.5	3.3 ± 0.1	314.6 ± 38.8	96.4 ± 15.5
ZZS-OSL-37	0.7	26.1 ± 5.0	26.8 ± 3.4	532.2 ± 0.2	3.0 ± 0.1	172.2 ± 8.0	57.2 ± 6.4
ZZS-OSL-38	5.0	39.3 ± 0.5	45.3 ± 3.2	537.1 ± 2.6	3.6 ± 0.1	170.4 ± 4.8	47.7 ± 5.1
ZZS-OSL-39	4.6	28.6 ± 3.8	45.6 ± 3.4	535.8 ± 3.5	3.5 ± 0.1	160.9 ± 6.6	45.7 ± 5.1
ZZS-OSL-40	2.4	40.6 ± 9.7	39.7 ± 8.3	523.7 ± 11	3.4 ± 0.1	142.0 ± 27.0	42.3 ± 9.1
ZZS-OSL-41	2.3	67.5 ± 1.9	51.5 ± 4.0	534.1 ± 0.6	4.2 ± 0.1	145.6 ± 3.0	35.0 ± 3.7
ZZS-OSL-42	2.2	61.5 ± 3.5	58.6 ± 2.1	606.5 ± 16	4.4 ± 0.1	130.7 ± 5.2	29.7 ± 3.3
ZZS-OSL-43	1.8	56.1 ± 0.6	53.5 ± 2.4	541.9 ± 4.4	4.1 ± 0.1	80.4 ± 7.0	19.5 ± 2.6
ZZS-OSL-44	1.6	55.8 ± 2.2	51.4 ± 2.7	525.2 ± 3.9	4.0 ± 0.1	138.2 ± 9.2	34.3 ± 4.2

(Continued on following page)

TABLE 1 (Continued) Result of OSL analysis for the layers in the trench.

	Depth (m)	U-238 (Bq/Kg)	Th-232 (Bq/Kg)	K-40 (Bq/Kg)	Dose rate (Gy/ka)	Equivalent dose (Gy)	OSL age (ka)
ZZS-OSL-45	1.2	67.0 ± 1.1	52.1 ± 2.1	510.4 ± 15	4.1 ± 0.1	104.3 ± 5.7	25.7 ± 3.0
ZZS-OSL-46	1.0	77.1 ± 0.3	64.6 ± 2.4	546.0 ± 2.6	4.7 ± 0.1	99.7 ± 6.0	21.0 ± 2.5
ZZS-OSL-51	1.7	29.7 ± 0.8	30.6 ± 2.5	524.4 ± 9.9	3.1 ± 0.1	98.1 ± 3.2	31.3 ± 3.4
ZZS-OSL-52	1.2	66.4 ± 15	50.7 ± 10.7	457.9 ± 0.5	3.9 ± 0.1	102.5 ± 2.3	26.1 ± 2.7
ZZS- 9	0.6	18.0 ± 2.0	30 ± 1.30	509 ± 9.51	3.1 ± 0.1	96.4 ± 1.6	31.5 ± 1.4
ZZS- 25	0.3	17.0 ± 2.6	28 ± 1.58	500 ± 6.36	3.32 ± 0.14	12.2 ± 0.3	3.7 ± 0.2
ZZS- 35	0.6	12.0 ± 0.9	34 ± 2.03	535 ± 9.51	3.08 ± 0.13	23.7 ± 0.5	7.7 ± 0.4

Geochronology of Institute of Disaster Prevention, China Earthquake Administration, by standard procedures for Chinese loess (Forman 1991; Wang, 2006). Fine-grain quartz fractions of 4–11 μm were obtained after a series of physical and chemical processes (Aitken, 1998). The equivalent doses were obtained based on the single-aliquot regenerative-dose (SAR) dating protocol (Wang, 2006). The determination of the environmental dose rate is also considered the standard rule (Aitken 1998; Wang, 2006). The dating information is listed in Table 1.

Paleoseismic observations and results

The northern segment of the ZWPF is composed of two left-step oblique faults (Figure 2). Trench 1 and trench 2 are located on the eastern side, and trench 3 is located on the western side (Figure 2).

Trench 1

Trench 1 and trench 2 are located on the flat alluvial fan far from the Zhuozi Shan. Based on the hillshade map interpretation and field investigation, in addition to the seasonal gullies, only one stage of alluvial fan development occurred around the trenches (Figure 3A). The fault traces cut the alluvial fan, which is clearly observed in the hillshade map and validated during field investigation (Figures 3A–C). DEM-based topographic profiles indicate that fault scarps at trench 1 and trench 2 sites are 2.0 ± 0.2 m and 2.6 ± 0.2 m, respectively (Figure 3D).

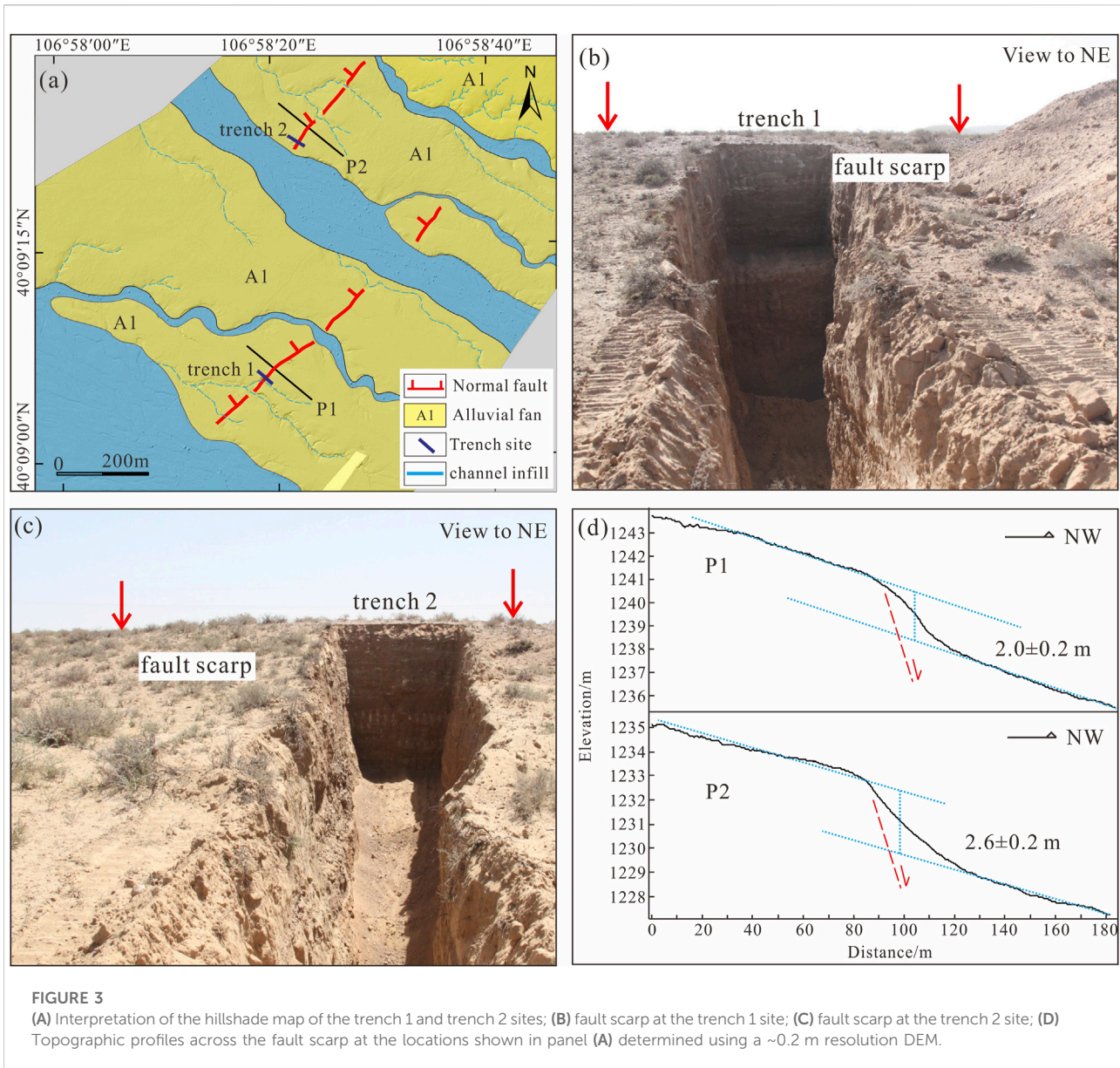
Faults can be easily identified according to the directional arrangement of gravel and the difference in strata on both sides of the faults plane in the mosaic photo of trench exposure (Figure 4). The three main faults (f1, f2, and f3) dip to the

west at dips of 63° – 67° , while McCaIpin, 2009 other secondary faults dip to the east.

The strata exposed by trench 1 can be divided into at least 15 units (Figure 4). All units are displaced except for unit U15 which covers the main deformation zone. Unit U1 comprises the footwall in the trench exposure, while units U2–U14 constitute the hanging wall. U1 is mainly composed of a light yellow sand gravel layer with nearly horizontal bedding and contains multiple fine sand layers, in which only developed at the foot wall. Two OSL samples collected from U1 yielded ages of 96.4 ± 15.5 ka and 57.2 ± 6.4 ka (Figure 4; Table 1). These ages are much older than those of the hanging wall strata. The footwall strata appear as regular deposits except for U5. U5 is a unit of gravel layers with a thickness of approximately 2 m. Four cycles of the rhythmic deposits are discernible from the trench mosaic picture and log (Figure 4). Every sedimentary sequence contains a lower gray loose layer (U2, U6, U9, and U12) and upper light red and hard buried paleosol layer (U3, U7, U10, and U13). Buried paleosols reflect the long-standing paleosurface environment and are also important indicators to identify paleoseismic events (Chen et al., 2003; Ran et al., 2014). U4 and U8 are interpreted as colluvial wedges, while U11 and U14 are interpreted as filling wedges. U4 does not have the characteristics of typical colluvial wedge mixed accumulation and may also be the gravel accumulation in the early stage of U5.

Based on the identified colluvial wedges, filling wedges and buried paleosol, four paleoseismic events in trench 1 are identified, named E1-1, E1-2, E1-3, and E1-4 from youngest to oldest. By dating the sediments formed before and after the earthquake, the corresponding lower and upper ages of seismic events can be obtained.

The timing of E1-4 may be after the formation of U3 but before that of U5. The ages of the two samples collected from U2 and U3 are relatively consistent, which are 45.7 ± 5.1 ka and 47.7 ± 5.1 ka, respectively. (Figure 4; Table 1). We use the age of 47.7 ± 5.1 ka from U3 as the lower bound of E1-4. A lack of

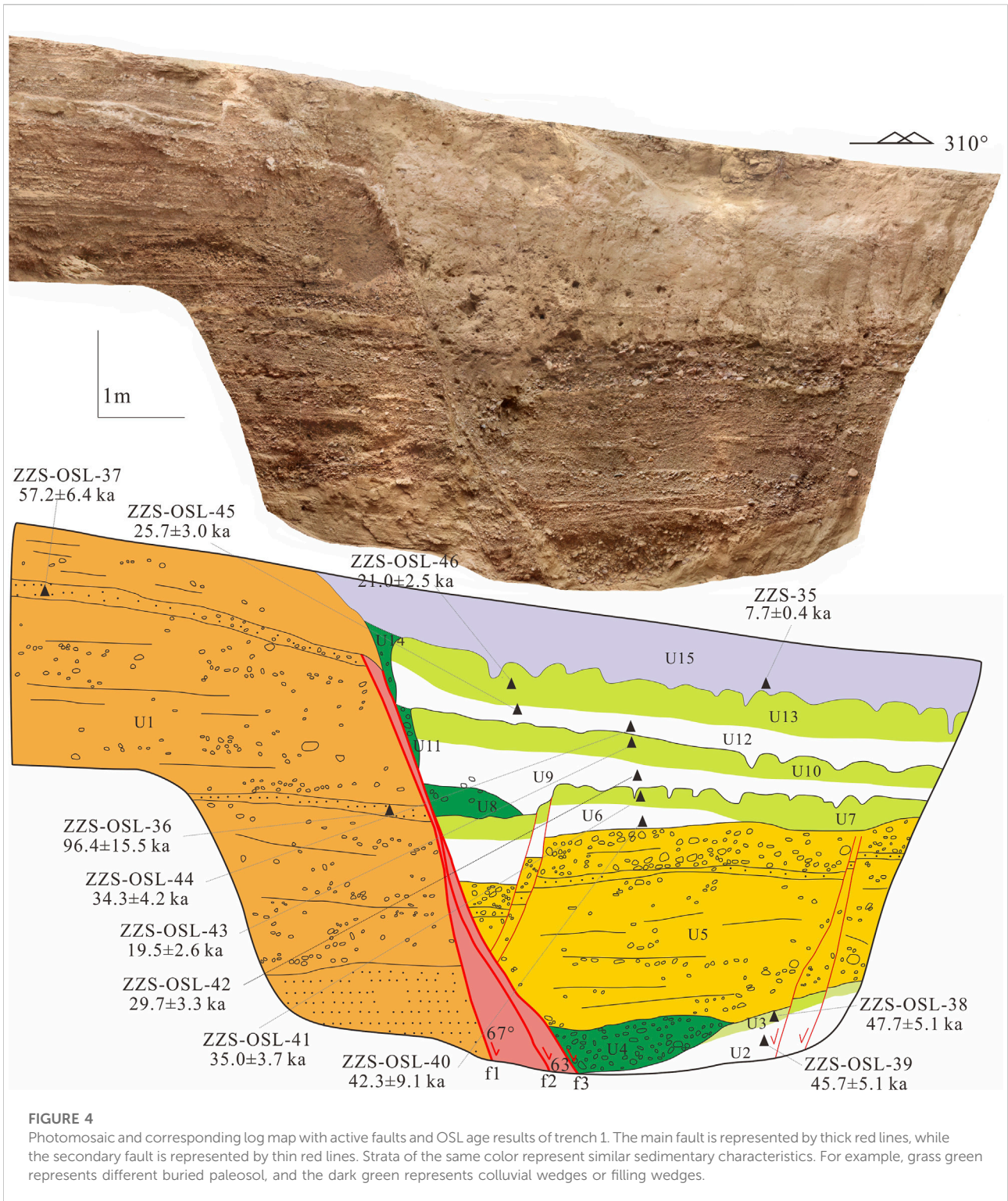


dateable material in U5 indicates that the timing of E1-4 cannot be accurately constrained. However, the sample collected from U6 can offer an upper bound age for E1-4. Thus, we roughly constrained that E1-4 occurred between 42.3 ± 9.1 ka and 47.7 ± 5.1 ka by dating U6 and U3 (Figure 4; Table 1). Two samples collected from U7 and U9 yielded ages of 35.0 ± 3.7 ka and 29.7 ± 3.3 ka, respectively (Figure 4; Table 1). These two ages provide the lower and upper bound ages for the occurrence of E1-3. The timing of E1-2 can be limited by samples from U12 and U10. However, the results of the ages are inverted and mismatched with the upper and lower units (Figure 4; Table 1). This may be related to incomplete bleached sediments or possible irregularities in the sampling process. Considering the ages and sedimentary relationship of the upper and lower units,

samples ZZS-OSL-45 and ZZS-OSL-42 are used to limit the timing of this event (Figure 4; Table 1). Thus, E1-2 is constrained to between 25.7 ± 3.0 ka and 29.7 ± 3.3 ka. E1-1 is the latest earthquake event that occurred on the fault. U14 is not faulted and is in sedimentary conformity with other strata. The samples collected from U15 and U13 constrain the timing of E1-1 to 7.7 ± 0.4 – 21.0 ± 2.2 ka (Figure 4; Table 1).

Trench 2

Three subparallel normal main faults, f1-f3, with dips of 62° – 73° to the west can be found in the trench based on stratigraphic correlation (Figure 5). Some secondary faults are



also distinguished (Figure 5). The strata can be classified into units U1–U16 from the field observations and mosaic picture of trench 2 (Figure 5). Units of U1–U4 are sand and gravel deposited units that formed in the early period. U5 is a buried paleosol that

experienced severe erosion. Then, it was covered by a loose U6 after an earthquake event. Similar to trench 1, trench 2 also contains three rhythmic sedimentary cycles; each cycle is composed of two units, U7 and U8, U9 and U10, and U12 and

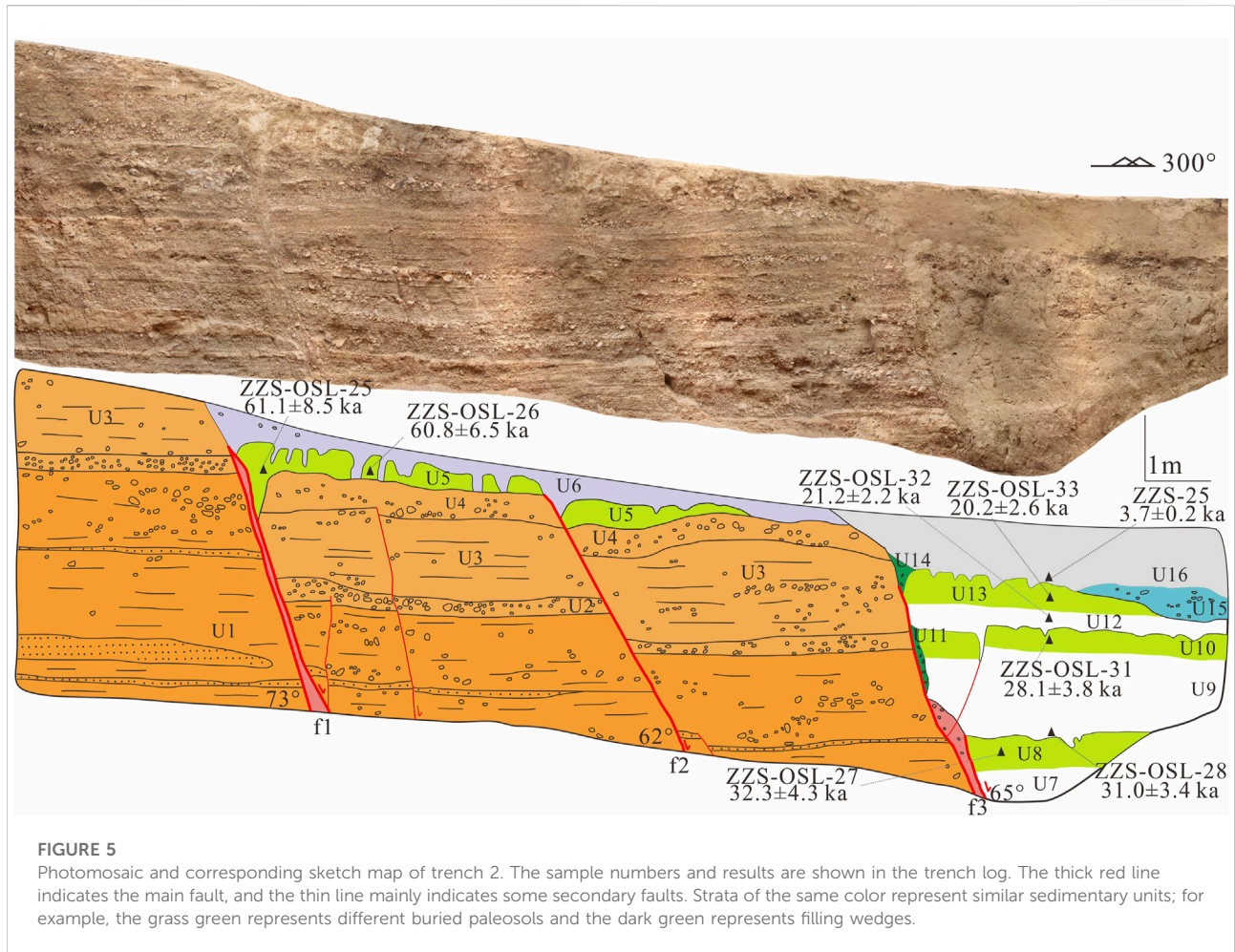


FIGURE 5

Photomosaic and corresponding sketch map of trench 2. The sample numbers and results are shown in the trench log. The thick red line indicates the main fault, and the thin line mainly indicates some secondary faults. Strata of the same color represent similar sedimentary units; for example, the grass green represents different buried paleosols and the dark green represents filling wedges.

U13, respectively (Figure 5). Among them, U7, U9, and U12 are paleosols, the surface has suffered a certain degree of erosion, and fissures have developed in them. U11 and U14 are interpreted as filling wedges, and U15 and U16 were deposited after the latest earthquake (Figure 5).

At least four earthquake events, named E2-1, E2-2, E2-3, and E2-4 from youngest to oldest, can be dated based on the colluvial wedges, filling wedges, and buried paleosol (Figure 5). In E2-4, f1 and f2 displaced units U1-U5 and were covered by U6. However, the fault throw on both sides of f1 is significantly greater than that of f2, which may indicate an earlier earthquake (Figure 5). Unfortunately, no other stratigraphic and sedimentary evidence remains.

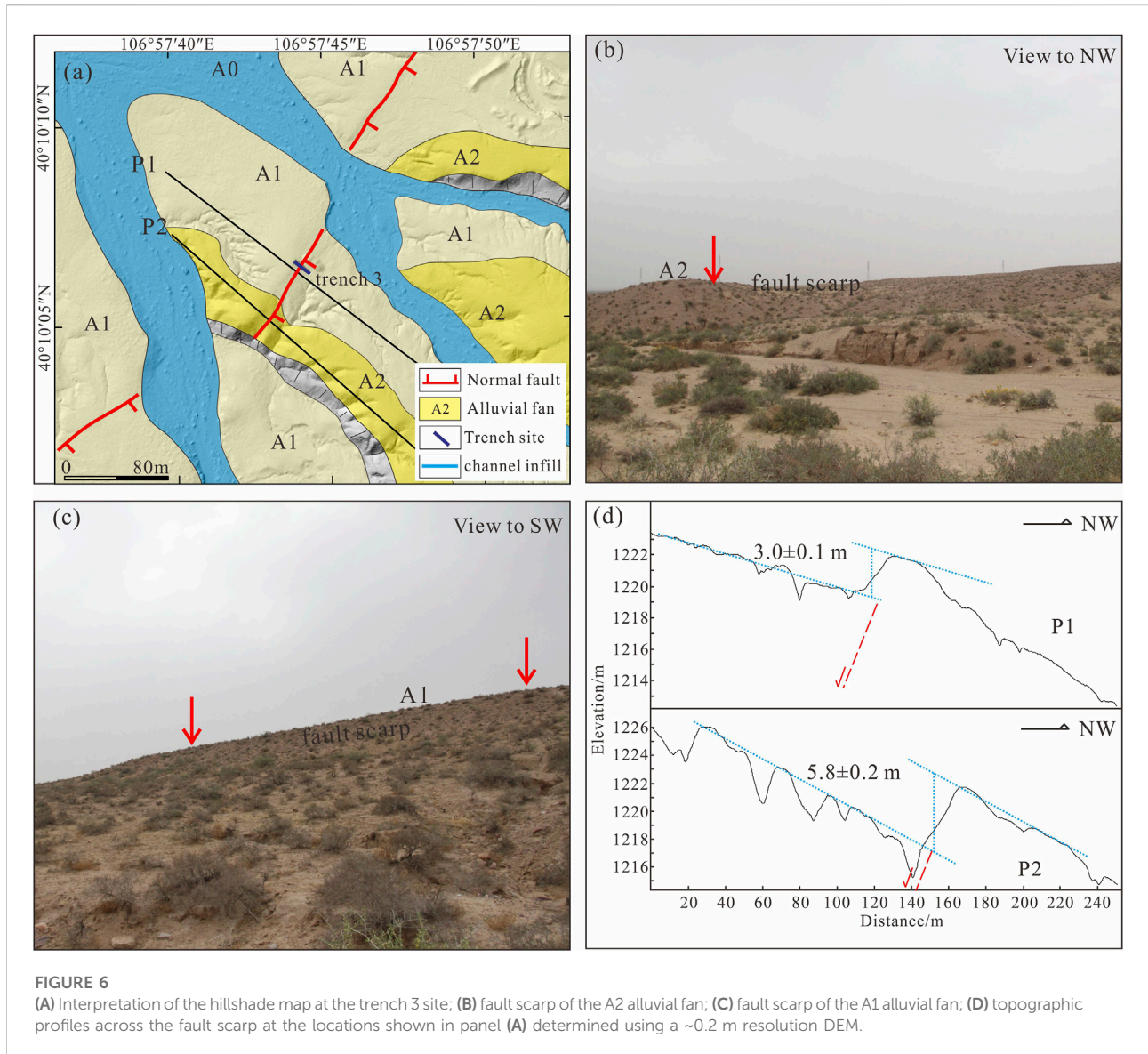
The formation ages of U5 and U6 can offer the lower and upper bound ages for E2-4. However, the thickness of U6 is too thin to be suitable for the collection of OSL samples. Two samples collected from U5 yielded ages of 61.8 ± 8.5 ka and 60.8 ± 6.5 ka (Figure 5; Table 1). Therefore, we suggest that E2-4 occurred after 60.8 ± 6.5 ka. The two samples from U9 and U8 constrain E2-3 to between 31.0 ± 3.4 ka and 32.3 ± 4.3 ka (Figure 5; Table 1). Based on two samples collected from U12 and U10, E2-2 can be constrained to

between 21.2 ± 2.2 ka and 28.1 ± 3.8 ka. The timing of the latest E2-1 is limited by samples ZZS-25 and ZZS-OSL-33, i.e., to between 3.7 ± 0.2 ka and 20.2 ± 2.6 ka (Figure 5; Table 1).

Trench 3

Trench 3 is located west of the trench 1 and trench 2 (Figure 2). A reverse dipping fault scarp is developed at the trench 3 site (Figure 6A). Two periods of alluvial fans are identified according to the hillshade map and field investigation (Figure 6A). Fault scarps dipping to the east are well preserved on alluvial fans A1 and A2 (Figures 6B,C). The scarp heights on the two alluvial fans are obviously different, reflecting the long-term continuous activity of the fault. The vertical throws determined from the DEM are approximately 3.0 ± 0.1 m and 5.8 ± 0.2 m, respectively (Figure 6D).

There are 21 stratigraphic units identified from the trench log as presented in Figure 7. U1 is mainly a set of yellowish brown sand gravel layers that can be found in both the hanging wall and



the footwall. According to the results of two samples (117.0 ± 14.0 ka and 91.1 ± 26.9 ka) of the intercalated fine sand layer (Figure 7; Table 1), the formation age of U1 is ca. 100 ka. Similar to trench 1 and trench 2, six cycles of rhythmic deposits are distinguished in trench 3 (Figure 7). Each cycle is composed of a buried paleosol in the upper part (U3, U6, U10, U13, U16, and U19) and loose sediments in the lower part (U2, U5, U9, U12, U15, and U18). U4 and U8 are interpreted as colluvial wedges, while U1, U14, U17, and U20 are interpreted as filling wedges. U21 was deposited after the latest earthquake and interpreted as an unfaulted unit (Figure 7).

A series of normal faults with different dips are in the ca. 8-m-wide deformation zone identified (Figure 7). The main faults, f1 and f2 which have opposite dips, form a small graben structure, in which many secondary faults are developed

(Figure 7). According to the stratigraphic correlation of the hanging wall and footwall, the cumulative displacement of f1 and f2 is approximately 5.2 m. The f3 and f4, which are nearly vertical and dip to the east, are developed on the east side of the trench. According to U3, the cumulative displacement of the two faults is approximately 1 m. The total cumulative displacement of strata is significantly greater than the height of the fault scarp, which may be due to the short measurement profile, which cannot remove the influence of scarp-derived deposit. According to the sedimentary characteristics of the strata and paleoseismic identification marks (Figure 7), six earthquake events, named E3-1, E3-2, E3-3, E3-4, E3-5, and E3-6 from youngest to oldest, can be determined from the trench.

The formation ages of U3 and U5 can offer the lower and upper bound ages for E3-6. The dating results of two samples

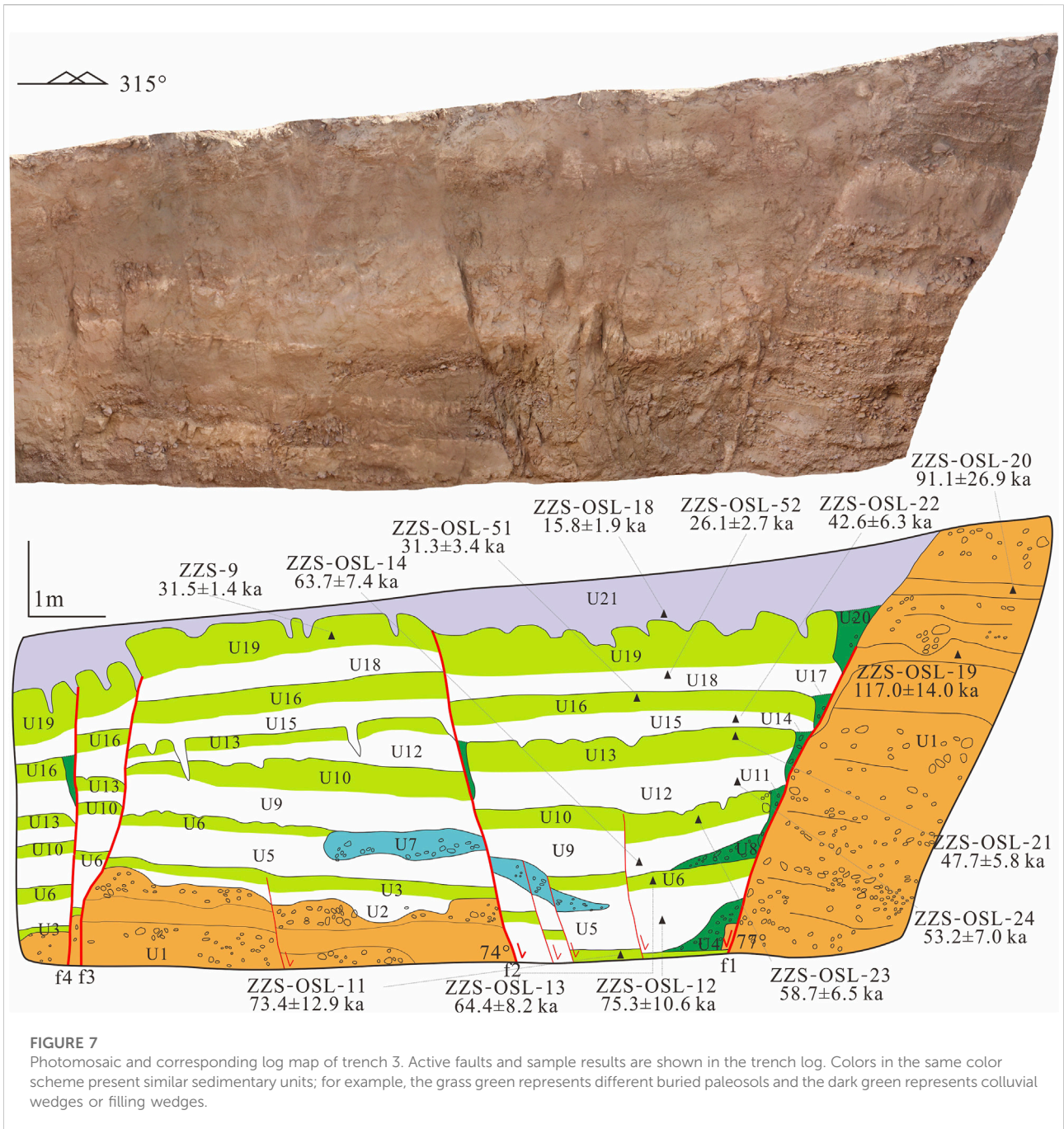
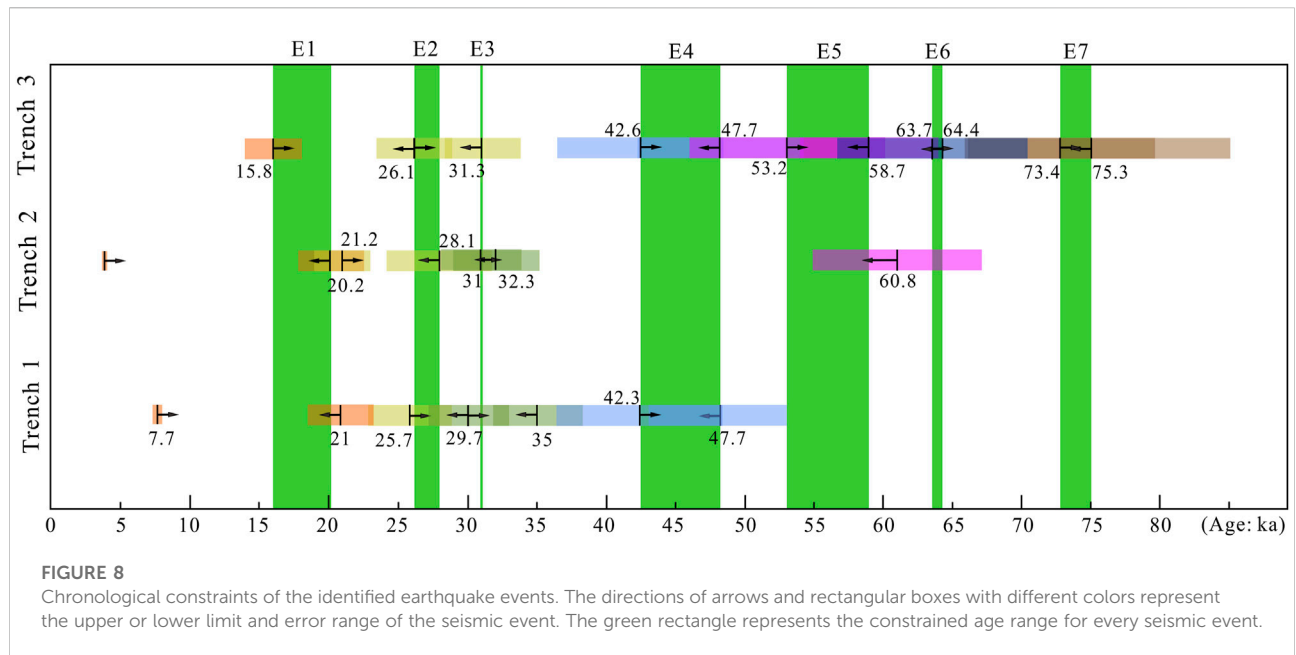


FIGURE 7 Photomosaic and corresponding log map of trench 3. Active faults and sample results are shown in the trench log. Colors in the same color scheme present similar sedimentary units; for example, the grass green represents different buried paleosols and the dark green represents colluvial wedges or filling wedges.

from U3 and U5 are 73.4 ± 12.9 ka and 75.3 ± 10.6 ka, respectively (Figure 7; Table 1). The results of the two samples are relatively consistent. Finally, the timing of E3-6 is determined to be between 73.4 ± 12.9 ka and 75.3 ± 10.6 ka. Two samples collected from U6 and U9 constrain the timing of the E3-5. The dating results yield ages of 64.4 ± 8.2 ka and 63.7 ± 7.4 ka for U6 and U9, respectively (Figure 7; Table 1). Therefore, the timing of E3-5 is between 64.4 ± 8.2 ka and 63.7 ± 7.4 ka.

The formation ages of U10 and U12 constrain the timing of E3-4 to between 53.2 ± 7.0 ka and 58.7 ± 6.5 ka (Figure 7; Table 1). Two filling wedges are developed in both E3-3 and E3-2 (Figure 7). The samples collected from U13, U15, U16, and U18 constrain the timing of E3-3 and E3-2 to 42.6 ± 6.3 - 47.7 ± 5.8 ka and 26.1 ± 2.7 - 31.3 ± 3.4 ka, respectively (Figure 7; Table 1). Filling wedge U20 is formed by sedimentation and is not faulted. Loose U21 formed after the earthquake and covered



U19, whose surface has been eroded. The timing of E3-1 should be constrained by the formation ages of U21 and U19. Sample ZZS-9 collected from U19 yields an age of 31.5 ± 1.4 ka, which is older than the underlying U18. By comprehensively comparing the age series of strata, we use the age of U18 as the lower bound of E3-1. Therefore, the timing of E3-1 is limited to between 15.8 ± 1.9 ka and 26.1 ± 2.7 ka (Figure 7; Table 1).

Discussion

Paleoseismic sequence of the zhuzishan west piedmont fault

The three trenches have revealed many earthquake events, some of which have large age ranges, or some have only the upper or lower age bounds. Using the progressive constraining method (Mao and Zhang, 1995), these events can be constrained to a narrow range to better discuss the recurrence and interval mode of paleoearthquakes. This method assumes that several trenches are excavated on a fault segment, and the number of events revealed by each trench is not exactly the same. However, there are always some events with similar ages in different trenches. Although some events determine only the upper or lower bound ages and some determine the range of the event ages, they may jointly constrain a time range for the events. Seven earthquake events, named E1 to E7 from youngest to oldest, can be determined from the 3 trenches by using the progressive constraining method (Figure 8).

The event E7 is only recorded in trench 3 and has an age range of 73.4 ± 12.9 ka to 75.3 ± 10.6 ka (Figure 8). This event

occurred early with big dating the error range. Therefore, it can be used as a reference for discussing seismic events.

The event E6 is also only found in trench 3, with an age between 63.7 ± 7.4 ka and 64.4 ± 8.2 ka (Figure 8). E6 and E7 are not recorded in trenches 1 and 2, which may be because the formation age of the landform at the sites of trenches 1 and 2 is younger than that of E6.

The event E5 is revealed in trench 2 and trench 3. Samples collected from U5 in trench 2 give the lower age bound of E5. However, this event can be constrained to a narrower range of 53.2 ± 7.0 ka to 58.7 ± 6.5 ka based on the dating results from trench 3 (Figure 8).

The evidence of event E4 is observed in trench 1 and trench 3. We infer that this event is also recorded in trench 2, if the hanging wall of main fault f3 was excavated deeper. Buried paleosol U3 in trench 1 and U13 in trench 3 show similar ages of ca. 47.7 ka (Figures 4, 7; Table 1), indicating that this may be the paleosurface existing at the same time. Finally, the occurring time of E4 is determined to be between 42.6 ± 6.3 ka and 47.7 ± 5.8 ka (Figure 8). Zhang (2014) reported that a paleoseismic event occurred in ca. 43.8 ± 4.6 ka in the southern segment of the ZWPF. We infer that they are the same event.

Evidence of rupture associated with the event E3 can be found in all trenches, which indicates the occurrence of E3. To constrain the age of E3, the formation age of buried paleosol U7 in trench 1, U8 in trench 2 and U16 in trench 3 are determined. The results of three samples from these units are 35.0 ± 3.7 ka, 32.3 ± 4.3 ka and 31.3 ± 3.4 ka, respectively (Figures 4, 5, 7; Table 1), which show consistency. The age result at the bottom of their upper unit is 31.0 ± 3.4 ka (Figure 5; Table 1). Thus, 31.0 ± 3.4 ka to 31.3 ± 3.4 ka can be considered to be the

timing of E3 (Figure 8). Notably, the age we determined for the timing of E3-2 is between 26.1 ± 2.7 ka and 31.3 ± 3.4 ka. Given these uncertainties, E3-2 can be assigned to either E2 or E3. However, given that U17 (the colluvial wedge) seems to extend and flatten from the top of U16, the bottom of U18 (capped above both U16 and U17) is relatively horizontal. The earthquake event represented by the formation of U17 may have an age closer to the U16, which is 31.3 ± 3.4 ka. Therefore, E3-2 should be assigned to event E3.

Clues of surface rupturing due to event E2 are observed only in trench 1 and trench 2. The dating results of the two samples for the penultimate period of the buried paleosol are quite different. The result of U10 in trench 1 is 19.5 ± 2.6 ka, and that of U10 in trench 2 is 28.1 ± 3.8 ka (Figures 4, 5; Table 1). According to the analysis of the dating results of the upper and lower stratigraphic units, we suggest that 28.1 ± 3.8 ka can better represent the formation age of the paleosol in this period. The dating result at the bottom of its upper unit is 26.1 ± 2.7 ka (Figure 7; Table 1). The timing of E2 is determined to be between 26.1 ± 2.7 ka and 28.1 ± 3.8 ka (Figure 8).

The event E1 is the most recent earthquake on the ZWPF, and was disclosed by TC1, TC2, and TC3. It faulted the latest buried paleosol and was covered by a loose sedimentary layer on the surface. Two samples collected from U13 in trenches 1 and 2 yield similar ages of 21.0 ± 2.5 ka and 20.2 ± 2.6 ka (Figures 4, 5; Table 1). Thus, we use the age of 20.2 ± 2.6 ka as the lower bound of the event. The ages of the loose surface sedimentary layer vary greatly, ranging from 3.7 ± 0.2 ka to 15.8 ± 1.9 ka (Figures 4, 5, 7; Table 1). The bottom age of 15.8 ± 1.9 ka can be used as the upper bound of the event. Therefore, the timing of E1 can be constrained to 15.8 ± 1.9 ka to 20.2 ± 2.6 ka (Figure 8). In the southern segment of the ZWPF, the age of the latest seismic event revealed by the trench is 20.0 ± 2.5 ka to 23.2 ± 2.5 ka, which may be the same event (Zhang, 2014).

In summary, we determine that the timing of seven paleoseismic events observed in the trenches on the ZWPF are 73.4 ± 12.9 ka to 75.3 ± 10.6 ka (E7), 63.7 ± 7.4 ka to 64.4 ± 8.2 ka (E6), 53.2 ± 7.0 ka to 58.7 ± 6.5 ka (E5), 42.6 ± 6.3 ka to 47.7 ± 5.8 ka (E4), 31.0 ± 3.4 ka to 31.3 ± 3.4 ka (E3), 26.1 ± 2.7 ka to 28.1 ± 3.8 ka (E2) and 15.8 ± 1.9 ka to 20.2 ± 2.6 ka (E1) (Figure 8).

Implications for the seismic hazard

Paleoseismic trenches are mainly located in the northern segment of the ZWPF. However, the study of paleoearthquakes is lacking in the middle and southern segments of the fault due to the lack of continuous fine-grained sediments and the influence of human activities. Studies have shown that two seismic events have occurred in the southern segment of the fault at ca. 20 ka and 43 ka (Zhang, 2014), which are more consistent with the two events revealed by the trench in the northern segment. These

results suggest that earthquake events have ruptured along the entire length of the fault. By applying the empirical relationships between moment magnitude (M_w) and surface rupture length (Wells and Coppersmith 1994), we take the equations for a normal fault as $M_w = 4.86 + 1.32 \times \log(\text{SRL})$. With a length of ~ 90 km, we obtain an M_w value of 7.4.

The total vertical displacement of the six seismic events revealed by trench 3 is approximately 6 m. Then, the average vertical displacement of each earthquake is inferred to be at least 1 m. There is no corresponding stratum in the hanging walls and footwalls of the faults in trench 1 and trench 2, so it is difficult to determine the total vertical displacement. The colluvial wedge formed by a single earthquake is generally half of the vertical displacement (Wallace, 1977; McCalpin, 2009). According to the height of colluvial wedge U8 in trench 1, it is inferred that the displacement of a single event is also ~ 1 m. The northern segment of the ZWPF is divided into two branches (Figure 2). The vertical displacement on each fault is approximately 1 m. Then, the total displacement of a single earthquake is approximately 2 m. Considering the fault dips of 70° , it is inferred that the coseismic displacement of each earthquake is approximately 2.2 m. In the middle segment of the ZWPF near Wuhai city, the height of the fault scarps formed on the geomorphic surface of ca. 20 ka is approximately 2.5 m (Gao, 2020). The coseismic displacement is inferred to be approximately 2.8 m based on the dip of 65° . Based on the empirical relationships between moment magnitude (M_w) and average displacement (Wells and Coppersmith 1994), we take the equations for a normal fault as $M_w = 6.78 + 0.65 \times \log(\text{AD})$. With an average displacement of 2.5 m, we obtain an M_w value of 7.0. Therefore, we suggest a preferred magnitude in the range of M_w 7.0 to M_w 7.4 for the ZWPF.

Seven paleoseismic events have been revealed in the northern segment of ZWPF. Considering the intermediate value of each earthquake event, the ages of each earthquake are 74.4 ka (E7), 64.1 ka (E6), 56 ka (E5), 45.2 ka (E4), 31.2 ka (E3), 27.1 ka (E2), and 18 ka (E1). Thus, the recurrence intervals of each earthquake are 10.3, 8.1, 10.8, 14, 4.1 and 9.1 ka, respectively. The relevant evidence for E2 is recorded only in trench 1 and trench 2. No evidence is found in trench 3, although it has a good sedimentary sequence. Meanwhile, no events having a similar time were found in the middle and southern segments of the fault (Zhang, 2014; Gao, 2020). When talking about the recurrence characteristics, we consider only the seismic events that ruptured the entire fault length. Thus, E2 can be excluded from the events list when calculating the recurrence interval. Then, the recurrence intervals of the remaining major earthquake events are 10.3, 8.1, 10.8, 14 and 13.2 ka, with a range of 8.1–14 ka.

Considering both the paleoseismic characteristics and the rupturing behavior of the ZWPF, a strong earthquake (M_w 7.0–7.4) may be caused by the ZWPF, which will generate a significant seismic hazard to Wuhai and adjacent areas in the

northwestern corner of the Ordos Block. As shown above, we conclude that the recurrence interval of strong seismic events in the ZWPF is 8.1–14 ka based on the paleoseismic sequence obtained in this study (Figure 8). Moreover, the most recent surface-rupturing event occurred at 15.8 ± 1.9 ka to 20.2 ± 2.6 ka, which suggests that the elapsed time in the ZWPF has approached or exceeded the recurrence interval of paleoearthquakes. Hence, we infer the ZWPF has a high seismic potential.

Conclusion

Based on the results of the analysis of paleoseismic trenches and OSL dating, we have obtained the following conclusions.

1) At least seven surface-rupturing earthquakes have occurred on the ZWPF since the late Pleistocene. The times of each earthquake are constrained to 73.4 ± 12.9 ka to 75.3 ± 10.6 ka (E7), 63.7 ± 7.4 ka to 64.4 ± 8.2 ka (E6), 53.2 ± 7.0 ka to 58.7 ± 6.5 ka (E5), 42.6 ± 6.3 ka to 47.7 ± 5.8 ka (E4), 31.0 ± 3.4 ka to 31.3 ± 3.4 ka (E3), 26.1 ± 2.7 ka to 28.1 ± 3.8 ka (E2) and 15.8 ± 1.9 ka to 20.2 ± 2.6 ka (E1). Furthermore, E2 is inferred to have been an event of lower magnitude that partially ruptured the fault, while other events are considered to be strong earthquakes that ruptured the entire length of the ZWPF.

2) Based on the paleoseismic event sequence of the ZWPF, the earthquake recurrence interval is estimated to be 8.1–14 ka. Compared with the most recent earthquake (E1), the elapsed time has approached or exceeded the recurrence interval. We infer that the ZWPF has a high seismic potential and will pose a significant seismic hazard in the western corner of the Ordos Block.

To better understand the seismogenic behavior and seismic hazard of the ZWPF, we suggest that further paleoseismic studies are needed in the middle and southern segments of the fault.

Data availability statement

The original contributions presented in the study are included in the article/supplementary material, further inquiries can be directed to the corresponding author.

References

- Aitken, M. J. (1998). *An introduction to optical dating: the dating of Quaternary sediments by the use of photon-stimulated luminescence*. Oxford University Press.
- Bemis, S. P., Micklethwaite, S., Turner, D., Mike, R. J., Akciz, S., Thiele, S. T., et al. (2014). Ground-based and UAV-based photogrammetry: A multi-scale, high-resolution mapping tool for structural geology and paleoseismology. *J. Struct. Geol.* 69, 163–178. doi:10.1016/j.jsg.2014.10.007
- Bi, H., Zheng, W., Ren, Z., Zeng, J., and Yu, J. (2017). Using an unmanned aerial vehicle for topography mapping of the fault zone based on structure from motion photogrammetry. *Int. J. Remote Sens.* 38, 2495–2510. doi:10.1080/01431161.2016.1249308
- Chen, L., Ran, Y., and Chang, Z. (2003). Characteristics of late Quaternary faulting and paleoseismic events on the east of Delingshan segment of the Seertengshan Piedmont Fault. *Seismol. Geol.* 25, 555–565.
- Deng, Q. (2002). Advances and overview on research of active tectonics in China. *Geol. Rev.* 48, 168–177.
- Deng, Q., and Liao, Y. (1996). Paleoseismology along the range-front fault of Helan mountains, north central China. *J. Geophys. Res.* 101, 5873–5893. doi:10.1029/95jb01814
- Deng, Q., Sung, F., Zhu, S., Li, M., Wang, T., Zhang, W., et al. (1984). Active faulting and tectonics of the Ningxia Hui Autonomous, China. *J. Geophys. Res.* 89, 4427–4445. doi:10.1029/jb089ib06p04427
- Dong, S., Zhang, P., Zheng, W., Yu, Z., Lei, Q., Yang, H., et al. (2018). Paleoseismic observations along the Langshan range-front fault, Hetao Basin, China: Tectonic and seismic implications. *Tectonophysics* 730, 63–80. doi:10.1016/j.tecto.2018.02.012

Author contributions

XL carried out field work, drew the figures and wrote the manuscript. ZG, QL, YS, and YY performed the fieldwork, samples collection, and aerial photogrammetry. All authors contributed to the manuscript and approved the submitted version.

Funding

This work was supported by the National Key Research and Development Program of China (2017YFC1500100) and the Innovation Team Project of the Earthquake Administration of Gansu Province (2019TD0101).

Acknowledgments

We greatly thank the reviewers and editors for their detailed comments and suggestions, which helped improve the manuscript.

Conflict of interest

The authors declare that the research was conducted in the absence of any commercial or financial relationships that could be construed as a potential conflict of interest.

Publisher's note

All claims expressed in this article are solely those of the authors and do not necessarily represent those of their affiliated organizations, or those of the publisher, the editors and the reviewers. Any product that may be evaluated in this article, or claim that may be made by its manufacturer, is not guaranteed or endorsed by the publisher.

- Du, J., Li, D., Wang, Y., and Ma, Y. (2017). Late Quaternary activity of the Huashan Piedmont Fault and associated hazards in the southeastern Weihe Graben, Central China. *Acta Geol. Sin. - Engl. Ed.* 91, 76–92. doi:10.1111/1755-6724.13064
- Feng, X., Ma, J., Zhou, Y., England, P., Parsons, B., Rizza, M. A., et al. (2020). Geomorphology and paleoseismology of the Weinan fault, Shanxi, Central China, and the source of the 1556 Huaxian earthquake. *JGR. Solid Earth* 125, e2019JB017848. doi:10.1029/2019JB017848
- Forman, S. L. (1991). Late Pleistocene chronology of loess deposition near Luochuan, China. *Quat. Res.* 36, 19–28. doi:10.1016/0033-5894(91)90014-V
- Gao, W., He, H., Zou, J., and Shi, F. (2017). The application of image-based modeling in paleoearthquake trench study. *Seismol. Geol.* 39, 172–182.
- Gao, Z. (2020). *Late Quaternary activity characteristics and risk analysis of large earthquakes of the Zhuozishan West Piedmont Fault*. Lanzhou, China: Lanzhou Institute of Seismology, China Earthquake Administration. Master Thesis.
- He, Z., Ma, B., Hao, Y., Zhao, J., and Wang, J. (2020). Surface rupture geomorphology and vertical slip rates constrained by terraces along the Wulashan Piedmont Fault in the Hetao basin, China. *Geomorphology* 358, 107116. doi:10.1016/j.geomorph.2020.107116
- Jiang, W., Deng, Q., Xu, X., and Xie, X. (2004). Surface rupture zone of the 1303 hongtong M=8 earthquake, Shanxi province. *Acta Seismol. Sin.* 26, 355–362.
- Jiang, W., Xiao, Z., and Xie, X. (2000). Segmentations of active normal dip-slip faults around Ordos Block according to their surface ruptures in historical strong earthquakes. *Acta Seismol. Sin.* 22, 517–526.
- Li, Y., Ran, Y., Chen, L., Wu, F., and Lei, S. (2015). The latest surface rupture events on the major active faults and great historical earthquakes in Hetao fault-depression zone. *Seismol. Geol.* 37, 110–125.
- Liang, K., Ma, B., Li, D., Tian, Q., Sun, C., He, Z., et al. (2019). Quaternary activity of the Zhuozishan West Piedmont Fault provides insight into the structural development of the Wuhai Basin and northwestern Ordos Block, China. *Tectonophysics* 754, 56–72. doi:10.1016/j.tecto.2019.02.004
- Lin, A., Rao, G., Hu, J., and Gong, W. (2013). Reevaluation of the offset of the Great Wall associated with the ca. M 8.0 Pingluo earthquake of 1739, Yinchuan Graben, China. *J. Seismol.* 17, 1281–1294. doi:10.1007/s10950-013-9391-2
- Liu, J., Yuan, Z., Xu, Y., Shao, Y., Wang, P., Xu, J., et al. (2021). Paleoseismic investigation of the recurrence behavior of large earthquakes on active faults. *Earth Sci. Front.* 28, 211–231.
- Ma, J., Feng, X., Li, G., Li, X., and Zhang, Y. (2016). The coseismic vertical displacement of surface rupture zone of the 1556 Huaxian earthquake. *Seismol. Geol.* 38, 22–30.
- Mao, F., and Zhang, P. (1995). Progressive constraining method in paleoseismic study and paleoearthquakes along the major active in northern Xinjiang. *Res. Act. Faults* (4), 153–164.
- McCalpin, J. M. (2009). *Paleoseismology*. Burlington, MA: Academic Press, 1–613.
- Meng, X., Yu, S., and Yi, Y. (1985). The investigation of deformation traces of Ms=8.0 earthquake in Hongdong, Shanxi province. *Seismol. Geol.* 7, 1–10.
- Middleton, T. A., Walker, R. T., Parsons, B., Lei, Q., Zhou, Y., and Ren, Z. (2016). A major, intraplate, normal-faulting earthquake: The 1739 Yinchuan event in northern China. *J. Geophys. Res. Solid Earth* 4, 293–320. doi:10.1002/2015JB012355
- Nie, Z., Wu, W., and Ma, B. (2010). Surface rupture of the A.D.849 earthquake occurred to the east of Baotou city, China, and discussion on its parameters. *Acta Seismol. Sin.* 32, 94–107.
- Ou, Q., Kulikova, G., Yu, J., Elliott, A., Parsons, B., and Walker, R. (2020). Magnitude of the 1920 Haiyuan earthquake reestimated using seismological and geomorphological methods. *JGR. Solid Earth* 125, e2019JB019244. doi:10.1029/2019JB019244
- Ran, Y., and Deng, Q. (1999). History, status and trend about the research of paleoseismology. *Chin. Sci. Bull.* 44, 880–889. doi:10.1007/bf02885057
- Ran, Y., Li, Y., Du, P., Chen, L., and Wang, H. (2014). Key techniques and several cases analysis in paleoseismic studies in mainland China (3): Rupture characteristics, environment impact and paleoseismic indicators on normal faults. *Seismol. Geol.* 36, 287–301.
- Rao, G., Chen, P., Hu, J., Yu, Y. L., and Qiu, J. (2016). Timing of Holocene paleo-earthquakes along the Langshan Piedmont Fault in the western Hetao graben, north China: Implications for seismic risk. *Tectonophysics* 677, 115–124. doi:10.1016/j.tecto.2016.03.035
- Rao, G., He, C., Cheng, Y., Yu, Y., Hu, J., Chen, P., et al. (2018). Active normal faulting along the Langshan Piedmont Fault, north China: Implications for slip partitioning in the western Hetao graben. *J. Geol.* 126, 99–118. doi:10.1086/694748
- Rao, G., Lin, A., and Yan, B. (2015). Paleoseismic study on active normal faults in the southeastern Weihe graben, Central China. *J. Asian Earth Sci.* 114, 212–225. doi:10.1016/j.jseas.2015.04.031
- Ren, Z., Zhang, Z., Chen, T., Yan, S., Yin, J., Zhang, P., et al. (2016). Clustering of offsets on the Haiyuan fault and their relationship to paleoearthquakes. *Geol. Soc. Am. Bull.* 128, B31155.1–18. doi:10.1130/b31155.1
- Research Group of Active Fault System around Ordos Massif (1988). *Active Fault system around Ordos Massif*. Beijing: Seismological Press, 1–352.
- Wallace, R. E. (1977). Profiles and ages of young fault scarps, north-central Nevada. *Geol. Soc. Am. Bull.* 88, 1267–1281. doi:10.1130/0016-7606(1977)88<1267:paaoyf>2.0.co;2
- Wang, X., Lu, Y., and Zhao, H. (2006). On the performances of the single-aliquot regenerative-dose SAR protocol for Chinese loess: Fine quartz and polymineral grains. *Radiat. Meas.* 41, 1–8. doi:10.1016/j.radmeas.2005.02.010
- Wells, D. L., and Coppersmith, K. J. (1994). New empirical relationships among magnitude, rupture length, rupture width, rupture area, and surface displacement. *Bull. Seismol. Soc. Am.* 84, 974–1002. doi:10.1007/BF00808290
- Xu, Y., He, H., Deng, Q., Allen, M. B., Sun, H., and Bi, L. (2018). The CE 1303 Hongdong earthquake and the Huashan Piedmont Fault, Shanxi graben: Implications for magnitude limits of normal fault earthquakes. *J. Geophys. Res. Solid Earth* 123, 3098–3121. doi:10.1002/2017JB014928
- Yang, X., Ran, Y., Hu, B., and Guo, W. (2002). Active fault and paleoearthquakes of the Piedmont Fault (Wuju-Mengkou-Dongfeng village) for Seerteng mountains, inner Mongolia. *Earthq. Res. China* 18, 127–140.
- Yang, X., Ran, Y., Hu, B., and Guo, W. (2003). Paleoseismic activity on Wujiage segment of Seerteng Piedmont Fault, inner Mongolia. *Acta Seismol. Sin.* 25, 62–71.
- Yu, Z., Yin, N., Wang, C., Deng, M., and Lan, W. (2021). Active tectonics, paleoseismology and seismic hazards of the piedmont Xizhoushan fault zone in the Shanxi graben system, north China Block. *J. Asian Earth Sci.* 205, 104590. doi:10.1016/j.jseas.2020.104590
- Zhang, B., Liao, Y., Guo, S., Wallace, R. E., Bucknam, R. C., and Hanks, T. C. (1986). Fault scarps related to the 1739 earthquake and seismicity of the Yinchuan graben, Ningxia Huizu Zizhiqu, China. *Bull. Seismol. Soc. Am.* 76, 1253–1287. doi:10.1785/bssa0760051253
- Zhang, G., Ma, H., Wang, H., and Li, L. (2004). Relationship between the active blocks in China and the strong seismic activity. *Sci. China (Ser. D)* 34, 591–599.
- Zhang, P., Deng, Q., Li, H., and Zhang, Z. (2013). Active faults, earthquake hazards and associated geodynamic process in continental China. *Sci. China (Ser. D)* 43, 1607–1620.
- Zhang, P., Deng, Q., Zhang, G., Ma, J., Gan, W., Min, W., et al. (2003). Active tectonic blocks and strong earthquakes in the continent of China. *Sci. China (Ser. D)* 33, 12–20.
- Zhang, P., Molnar, P., Zhang, W., Deng, Q., Wang, Y., Burchfiel, B. C., et al. (1988). Bounds on the average recurrence interval of major earthquakes along the Haiyuan fault in north-central China. *Seismol. Res. Lett.* 59, 81–89. doi:10.1785/gssr.59.3.81
- Zhang, P., Wang, Q., and Ma, Z. (2002). GPS velocity field and active crustal blocks of contemporary tectonic deformation in continental China. *Earth Sci. Front.* 9, 430–441.
- Zhang, Y. (2014). *Late Quaternary activity of the Zhuozishan Western Piedmont Fault*. Beijing, China: Institute of Crustal Dynamics, China Earthquake Administration. Master Thesis.
- Zheng, W., Wang, Q., Yuan, D., Zhang, D., Zhang, Z., and Zhang, Y. (2020). The concept, review and new insights of the active tectonic block hypothesis. *Seismol. Geol.* 42, 287–301.
- Zheng, W., Zhang, P., Yuan, D., Wu, C., Li, Z., Ge, W., et al. (2019). Basic characteristics of active tectonics and associated geodynamic processes in continental China. *J. Geomech.* 25, 699–721.